ISSN: 2096-3246
Volume 58, Issue 01, 2026

EFFECT OF LANTHANUM NANOPARTICLES ON THE RADIATION ATTENUATION PROPERTIES OF LITHIUM ZINC TELLUROBORATE GLASSES

Kiran Nagaraju , Susheela K Lenkennavar [*]
kirannagaraju@bub.ernet.in & susheelakl@bub.ernet.in
Department of Physics, Bangalore University, Bengaluru, Karnataka, 560056, India.

Abstract :
In this study, Lithium Zinc telluroborate glasses incorporated with Lanthanum nanoparticles (LZTBLn) were prepared using the conventional melt-quenching method. The density and molar volume of the glasses were calculated. XRD analysis confirmed that all samples are amorphous in nature. The radiation shielding ability of the glasses was evaluated using computational simulation technique. Shielding parameters such as the Linear attenuation coefficient (LAC), Mass attenuation coefficient (MAC), Effective atomic number (Z_{eff}), Half-value layer (HVL), Tenth-value layer (TVL), and Mean free path (MFP) were determined over a wide range of photon energies (0.015-15MeV). The results show that increasing the La_2O_3 nanoparticles content improves the radiation shielding performance than other traditional shielding materials. These findings suggest that La_2O_3 doped lithium zinc telluroborate glasses are promising, lightweight, and non-toxic materials for radiation shielding applications.
Keywords: Lanthanum Nanoparticles, XRD, Linear and Mass attenuation coefficients.

1.Introduction:

Over the last few decades, new and innovative technologies have been developed to support the requirements of mankind. It is clear that nuclear technology is one of the technologies employed across multiple domains, including radiation therapy in the medical field, elemental analysis, nuclear energy plants, space technology, and medical physics. Despite the advantages of this power, its implementation in real-world applications leads to the production of numerous harmful radiations, such as γ-rays, neutrons, and electrons from various origins, including nuclear power stations, nuclear weaponry, healthcare centres, diagnostic facilities, and health research labs, which is unfortunate [1-3]. The capacity for gamma radiation to penetrate is largely a result of its significant energy and minuscule wavelength [4]. Continuous exposure to these types of ionizing radiation for an extended period can result in severe health complications such as skin eruptions, bone marrow problems, radiation syndrome, tissue destruction, mental stress, genetic disorders, cancer, and potentially sudden death [5]. Due to the significant growth in the use of intense radiation across different fields, it is crucial to ensure the safety of society and the environment from these radiations, which inspires researchers to seek out new shielding materials. Many research groups are exploring new and high-quality shielding materials to minimize radiation to safe and acceptable levels [6-8]. Selecting the appropriate and efficient radiation shielding materials is a significant consideration that relies on the requirements and implementation or usage. To achieve radiation suppression, radiation shielding components must be produced with high density, substantial stability, good radiation attenuation, low toxicity, and ease of preparation. Key materials for radiation shielding consist of concrete blocks, tiles, and clay bricks. These materials act as barriers, significantly reducing radiation to non-harmful levels due to their dense composition, cost-effectiveness, and versatility [9-11]. Materials like ceramics [12], glasses [13], polymers [14] and alloys [15] have been investigated as suitable shielding materials. Among all materials, glasses are regarded as the most suitable option for shielding applications due to their remarkable attributes such as excellent transparency, stability, high hardness, compositional resilience, cost-effectiveness, and ease of preparation using various methods [16–18].

The capabilities of borate glasses are enhanced by incorporating rare-earth elements such as lanthanum oxide (La_2O_3). Lanthanum oxide, recognized for its ability to improve the density and stability of glass, plays a significant role in the overall performance of the material, particularly in situations where radiation shielding and durability are essential [19,20]. The capability of borate-based glasses, especially when integrated with the synergistic effects of ZnO and La_2O_3, has made it possible to develop materials that are excellently suited for high-demand technological applications [21]. The addition of La_2O_3 to the TeO_2-ZnO glass system indicated higher hardness values and improved material properties [22]. Alkali oxides such as Li_2O when added to borate glasses, lowers its viscosity and aid in formation of glasses [23]. The focus of the current research is to evaluate the effectiveness of radiation shielding in glass samples of Lithium zinc telluroborate that have been doped with lanthanum oxide nanoparticles. In order to achieve this significant radiation shielding parameters have been analysed with the help of Photon Shielding and Dosimetry (PSD) software (Phy-X/PSD) [24].

2.Materials and Methods:

2.1 Experimental: The Quinary glass system with chemical composition of $15Li_2O$-25ZnO-$2TeO_2$- (58-x) B_2O_3-xLa_2O_3 Nps (x varying between 0 and 0.4 in steps of 0.1 mol%), were synthesized via the conventional melt-quenching method and are labeled as LZTBLn-0, LZTBLn-0.1, LZTBLn-0.2, LZTBLn-0.3, LZTBLn-0.4 for x=0, 0.1,0.2, 0.3, and 0.4 mol% respectively. The materials used consisted of high-purity of Li_2O, TeO_2, ZnO, H_3BO_3, and La_2O_3 nanoparticles. The concentration of La_2O_3 was varied and substituted in place of B_2O_3. The full batch was mixed in order with set quantities of ZnO, Li_2O, and TeO_2. The homogeneous mixed powders were transferred into a porcelain crucible, which was then placed in a muffle furnace for melting at 900 °C for 2 hours, after which they were quenched onto a brass plate. Thermal annealing of the quenched glasses was performed at 300 °C for 3 hours to release the internal stress present in the samples. At last, we were brought to room temperature and were polished to the required dimensions for additional measurements and it is represented in **Fig. 1**. The measurement of density (ρ) was conducted with toluene as the immersion liquid, determined through Archimedes' principle at room temperature. The thickness of the glass samples was measured using a screw gauge. The amorphous properties of the glasses were validated using the Rigaku x-ray diffractometer.

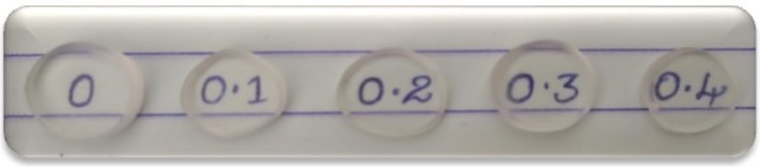

Fig. 1 Prepared LZTBLn glass samples

2.2 Computational: The Phy-X/PSD computational tool is a significant resource for determining the radiation shielding properties of glass materials [25]. It delivers theoretical calculations of important parameters such as mass attenuation coefficient (MAC) (cm^2/g), linear attenuation coefficient (LAC) (cm^{-1}), mean free path (MFP) (cm), half-value layer (HVL) (cm), and tenth-value layer (TVL) (cm) across a wide range of energies. Through the application of fundamental models, including the Beer–Lambert law and the mixture rule, it accurately simulates photon interactions in complex glass matrices. Phy-X/PSD also determines the effective atomic number (Z_{eff}), which gives insights into how well glasses with heavy metal oxides shield against radiation. This facilitates researchers in optimizing glass formulations for radiation shielding applications ahead of experimental validation. Its user-friendly nature and comprehensive results render it a crucial resource in the advancement of high-performance shielding materials [26-27]. The attenuation of photons in a material is determined by the Beer–Lambert law, which is expressed as

$I = I_0 e^{-\mu x}$ ………. (1)

Where I and I_o are the incident and transmitted photon intensities, respectively, μ is the linear attenuation coefficient (LAC) (cm^{-1}), and x is the thickness of the material (cm). This exponential law demonstrates the chance of photons being absorbed or scattered within the medium, with an increased μ indicating superior shielding capability [28].

In order to compare various materials or compositions, it is usual to normalize μ by the density ρ, yielding the mass attenuation coefficient (MAC). Where ρ is the density of the material (g/cm^3). Half Value Layer (HVL) denotes the thickness of a substance necessary to cut down the intensity of incoming radiation (commonly gamma or X-rays) to half of its original value. A smaller HVL is a direct indicator of a material's shielding effectiveness, suggesting that it has better shielding capabilities. Tenth Value Layer (TVL) represents the thickness of a material that is required to cut down the intensity of incident radiation to 10% of its original intensity. In safety calculations, TVL is particularly significant when high-level shielding is essential, as seen in radiotherapy rooms and nuclear facilities. Mean Free Path (MFP) indicates the average distance a photon travels within a material before it interacts. It is computed as the reciprocal of the linear attenuation coefficient. A lower mean free path (MFP) reflects a higher chance of interaction and superior shielding performance. Materials with high-Z elements in glass systems help reduce MFP, thereby improving radiation protection [29-30].

$MAC = \frac{\mu}{\rho}$ ………. (2)

$HVL = \frac{\ln 2}{\mu} = \frac{0.693}{\mu}$ ………. (3)

$TVL = \frac{\ln 10}{\mu} = \frac{2.302}{\mu}$ ………. (4)

$MFP = \frac{1}{\mu}$ ………. (5)

The Effective Atomic Number (Z_{eff}) serves as a parameter that indicates the total atomic number of a composite material, treating it as if it were a single-element substance. It considers the role of each individual element according to its atomic number, weight fraction, and electron interaction characteristics. Z_{eff} plays a vital role in radiation shielding research as it affects the interaction of photons with the material. Higher Z_{eff} values typically result in increased photoelectric absorption, particularly at lower photon energies. In advanced glass systems, calculating Z_{eff} is crucial for prediction and comparison of their photon attenuation efficiency. Where σ_a is the total atomic cross-section and σ_e is the total electronic cross-section [31].

$$Z_{eff} = \frac{\sigma_a}{\sigma_e} \quad \text{.........} (6)$$

The Total Atomic Cross Section (σ_a) and Total Electronic Cross Section (σ_e) serve as crucial parameters for analyzing how the interaction of photons with matter, particularly in composite materials such as glasses or nanocomposites. Total Atomic Cross Section (σ_a) denotes the effective area that all atoms in a substance present to an incoming photon beam for interaction. It considers the total probabilities of photon interactions, including photoelectric absorption, Compton scattering, and pair production. It is calculated using the mass attenuation coefficient (MAC), the atomic weight (A_i), and Avogadro's number (N_A), W_i is the weight fraction, Z_i is the atomic number, f_i is the fractional abundance of element i. Total Electronic Cross Section (σ_e), this quantifies how likely a photon will interact with an electron in the material. The elemental composition of the sample is involved, where each element contributes based on its atomic number and abundance [32].

$$\sigma_e = \frac{1}{N_A} \sum_i f_i A_i \, (MAC)_i \quad \text{.........} (7)$$

$$\sigma_e = \frac{1}{N_A} \sum_i \left(\frac{f_i A_i}{Z_i}\right) (MAC)_i \quad \text{.........} (8)$$

3.Result and discussion:

3.1 X-ray Diffraction (XRD): The XRD spectra of the synthesized glasses like Base glass (LZTBLn-0) and high concentration of La_2O_3 glass (LZTBLn-0.4) shown in **Fig. 2**, were recorded at angles between 20° and 80°.The absence of sharp peaks, along with the existence of a large hump, indicates long-range structural instability, which suggests that the synthesized glasses are amorphous in nature [33].

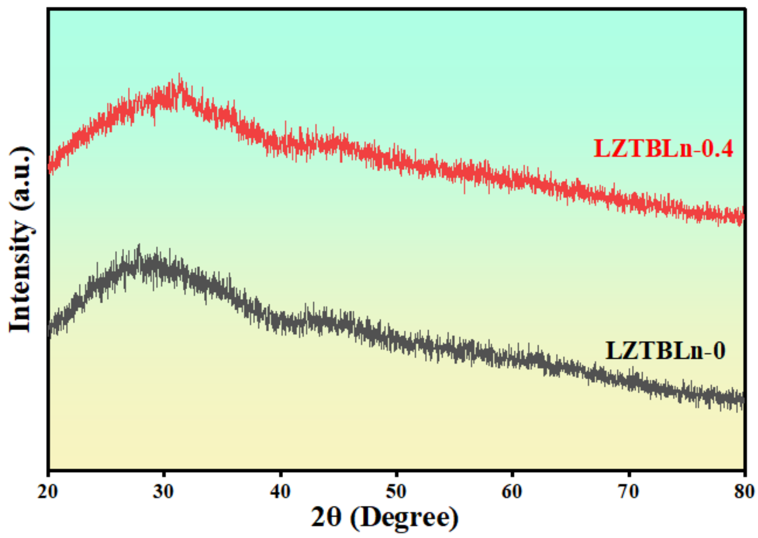

Fig. 2. X-ray diffraction patterns of synthesized LZTBLn glass samples

3.2 Physical Parameters: To improve our understanding of the influence of La_2O_3 Nps on the glass network, we calculated and analysed the density, molar volume, and other physical parameters of LZTBLn glasses. The density (ρ) and Molar volume (V_m) of the glass samples can be obtained by using the following formulas:

$$\rho = \left(\frac{Wa}{Wa-Wb}\right)\ \rho_b \qquad \dots\dots\dots \qquad (9)$$

$$V_m = \frac{MW}{\rho} \qquad \dots\dots\dots \qquad (10)$$

Here, W_a and W_b indicate the weight of glass in air and in toluene, respectively. The density of toluene is represented by ρ_b, and MW stands for the molecular weight of the glass. **Fig. 3** displays a graphical representation of density and molar volume. Furthermore, the and Concentration (N_i) ions/cm^3, Polaron radius (r_p) nm, Inter ionic distance (r_i) nm, Field strength (F) nm^{-2} are calculated using formulas [34] and Using a screw gauge, the thickness of the glass samples was evaluated are listed in **Table. 1** below.

Glass Samples	M.W (g/mol)	(ρ) g/cm^3	V_m (cm^3/mol)	N_i (10^{19})(ions/cm^3)	r_p (nm)	r_i (nm)	F (10^{18}) nm^{-2}	Thickness (cm)
LZTBLn -0	68.39	2.799	24.43	-	-	-	-	0.351
LZTBLn - 0.1	68.67	2.853	24.06	5.00	1.093	2.713	2.508	0.256
LZTBLn - 0.2	68.94	2.855	24.14	9.97	0.868	2.156	3.973	0.225
LZTBLn - 0.3	69.21	2.866	24.14	14.96	0.759	1.883	5.206	0.314
LZTBLn - 0.4	69.49	2.869	24.22	19.89	0.690	1.713	6.294	0.216

Table. 1. Physical Parameters of LZTBLn glasses

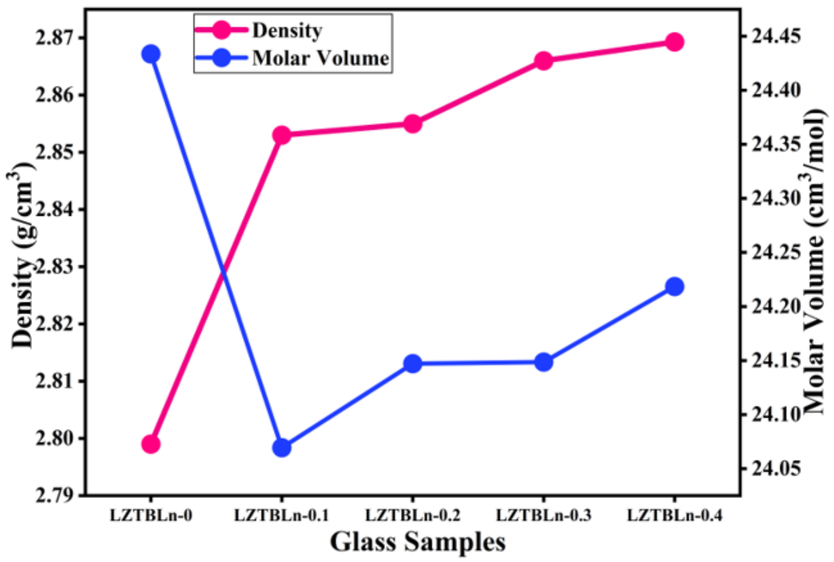

Fig. 3 Density vs Molar Volume of synthesized LZTBLn glass samples

The physical and structural characteristics of the LZTBLn glass system exhibit a consistent alteration as the concentration of La_2O_3 increases, signifying a gradual modification and compaction of the glass network. From LZTBLn-0 to LZTBLn-0.4, there is a consistent increase in molecular weight and density, resulting from the incorporation of lanthanum ions and the improved packing efficiency of the glass matrix [35-36]. Incorporating La_2O_3 results in a reduction of molar volume, suggesting a decrease in free space and a denser glass structure. As doping increases, the concentration of lanthanum ions also rises, resulting in a decrease in the polaron radius and inter-ionic distance, which indicates tighter packing of the ions and enhanced interactions. The steady increase in field strength implies that La-O bonds are strengthening, which also enhances the electrostatic interaction between the modifier ions and the glass structure. The findings collectively suggest that La_2O_3 serves as an efficient network modifier, leading to a telluroborate glass that demonstrates enhanced density and compactness, as well as superior structural properties [37].

3.3 Radiation Shielding Properties:

3.3.1. Mass attenuation coefficient (MAC): The prepared LZTBLn glasses (MAC) values were measured in the photon energy range of 0.015-15 MeV, which are listed in **Table. 2**. Compering with ordinary concrete and hematite-serpentine, it indicates a gradual decrease with higher photon energy, a trend that is representative of gamma-ray interaction mechanisms [38]. A similar trend was seen in every glass composition. Many other glasses have reported a trend where MAC values decrease from higher to lower levels [39-41]. In the low energy region (0.015-0.05 MeV), the MAC values are very high. at 0.015 MeV, the MAC values of LZTBLn glasses range from 22.325 to 23.072 cm^2/g, which are much higher than ordinary concrete (7.079 cm^2/g) and also higher than hematite-serpentine (21.54 cm^2/g). This high attenuation is due to the dominance of the photoelectric effect, which strongly depends on atomic number. In the intermediate energy region (0.1-1 MeV), the MAC values decrease significantly. At 0.5 MeV, the MAC values of the prepared glasses are around 0.085 cm^2/g, which are comparable but still slightly better than ordinary concrete and hematite–serpentine. This reduction occurs because Compton scattering becomes the dominant interaction mechanism, and it depends mainly on electron density rather than atomic number. In the high energy range from above 1 MeV up to 15 MeV, the MAC values decrease slowly and become nearly constant. At 15 MeV, the values range from about 0.022-0.023 cm^2/g for the prepared glasses, while ordinary concrete and hematite–serpentine show slightly higher values. Although pair production contributes at higher energies, the overall interaction probability is lower than at low energies, resulting in small MAC values. Among all compositions, LZTBLn-0.4 shows the highest MAC values, especially in the low energy range, Overall, the results confirm that the prepared LZTBLn glasses, particularly those with higher La_2O_3 content, possess promising radiation shielding characteristics compared to conventional shielding materials. Glass with largest amount of lanthanum oxide showed maximum MAC values [42-43]. This trend is shown in **Fig. 4**

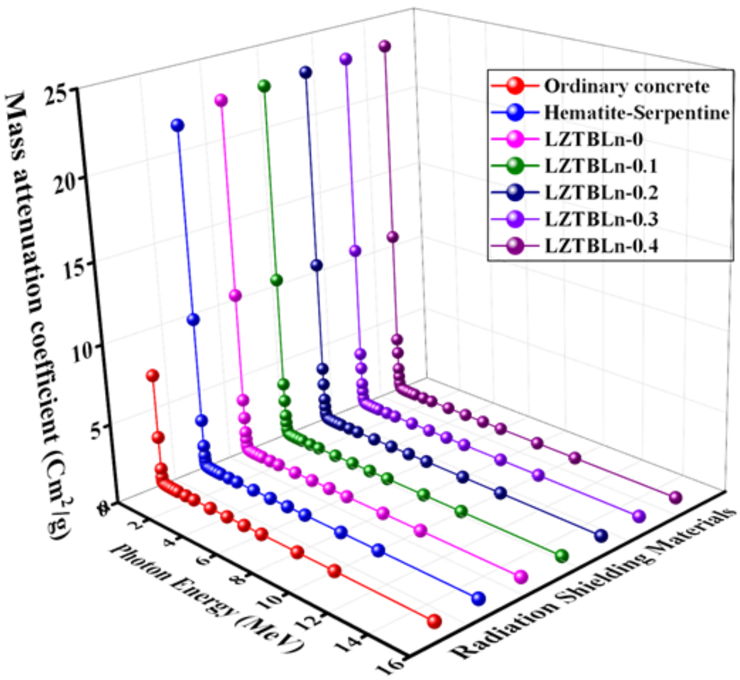

Fig. 4. Variation of Mass attenuation coefficient (MAC) with incident photon energy for Radiation shielding materials

.

Photon energy (MeV)	MAC (cm^2/g)						
	Ordinary concrete	Hematite-Serpentine	LZTBLn-0	LZTBLn-0.1	LZTBLn-0.2	LZTBLn-0.3	LZTBLn-0.4
0.015	7.079	21.54	22.325	22.514	22.702	22.888	23.072
0.02	3.105	9.661	10.264	10.352	10.439	10.526	10.612
0.03	1.048	3.124	3.413	3.443	3.473	3.502	3.531
0.04	0.5415	1.443	2.226	2.322	2.418	2.512	2.606
0.05	0.3584	0.8261	1.262	1.316	1.369	1.422	1.475
0.06	0.2417	0.5475	0.814	0.847	0.880	0.913	0.945
0.08	0.2043	0.3192	0.438	0.453	0.468	0.483	0.498
0.1	0.1725	0.2328	0.295	0.303	0.311	0.319	0.327
0.15	0.1427	0.1591	0.176	0.179	0.181	0.184	0.186
0.2	0.1271	0.1333	0.139	0.140	0.141	0.142	0.143
0.3	0.1086	0.1096	0.109	0.109	0.110	0.110	0.110
0.4	0.09677	0.09646	0.095	0.095	0.095	0.095	0.095
0.5	0.08816	0.08744	0.085	0.085	0.085	0.085	0.086
0.6	0.07992	0.08058	0.078	0.078	0.078	0.078	0.078
0.8	0.07144	0.07052	0.068	0.068	0.068	0.068	0.068
1	0.0642	0.0633	0.061	0.061	0.061	0.061	0.061

1.5	0.05227	0.05154	0.050	0.050	0.050	0.050	0.050
2	0.04507	0.0456	0.043	0.043	0.043	0.043	0.043
3	0.03668	0.03667	0.035	0.035	0.035	0.035	0.035
4	0.03195	0.03236	0.031	0.031	0.031	0.031	0.031
5	0.02894	0.02969	0.028	0.028	0.028	0.029	0.029
6	0.0269	0.02795	0.027	0.027	0.027	0.027	0.027
8	0.02436	0.02589	0.025	0.025	0.025	0.025	0.025
10	0.02291	0.02482	0.023	0.023	0.024	0.024	0.024
15	0.02122	0.02382	0.022	0.022	0.022	0.023	0.023

Table. 2. Calculated values of Mass Attenuation Coefficients using Phy-X/PSD software

3.3.2. Linear attenuation coefficient (LAC): The linear attenuation coefficient (LAC) values of the prepared LZTBLn glasses were analysed over the photon energy range of 0.015-15 MeV is tabulated in **Table. 3**. In the very low energy region (0.015-0.05 MeV), the LAC values are extremely at 0.015 MeV, the values range from about 62.287 cm^{-1} (LZTBLn-0) to 66.195 cm^{-1} (LZTBLn-0.4), whereas ordinary concrete and hematite-serpentine show much lower values of 16.28 cm^{-1} and 53.85 cm^{-1}, respectively. This high attenuation in the low energy region is mainly due to the dominance of the photoelectric effect, which strongly depends on atomic number and density. In the intermediate energy region (0.1-1 MeV), the LAC values decrease sharply for instance, at 0.5 MeV, the values for the prepared glasses fall to around 0.238-0.245 cm^{-1}, where Compton scattering becomes the dominant interaction mechanism and attenuation depends mainly on electron density. In the high energy region (above 1 MeV up to 15 MeV), the LAC values further decrease and tend to vary slowly, with values around 0.062–0.065 cm^{-1} at 15 MeV, indicating the contribution of pair production along with reduced overall interaction probability. [43-45]. Also, a continuous increase in LAC is observed as the lanthanum oxide content rises across all energy ranges, with LZTBLn-0.4 consistently showing the highest values. This enhancement is due to greater atomic number and density of lanthanum, which improves photon interaction. Compared to ordinary concrete and hematite–serpentine, the prepared LZTBLn glasses demonstrate superior attenuation performance, particularly in the low energy region, confirming their suitability as effective radiation shielding materials, we can observe the trend in **Fig. 5**.

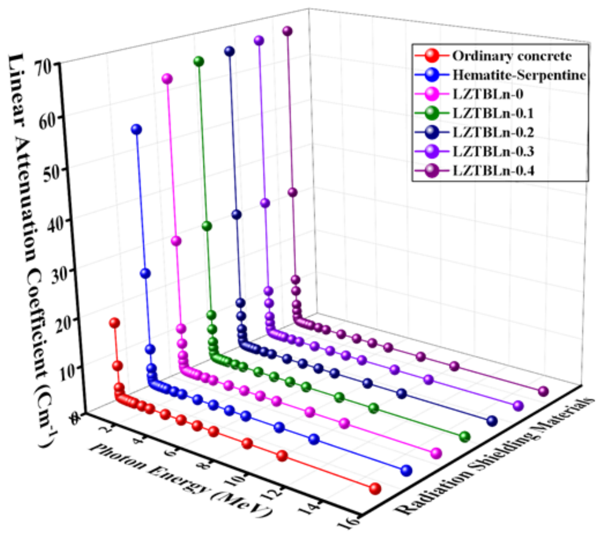

Fig. 5. Variation of Linear attenuation coefficient (LAC) with incident photon energy for Radiation shielding materials

Photon energy (MeV)	LAC (cm^{-1})						
	Ordinary concrete	Hematite-Serpentine	LZTBLn-0	LZTBLn-0.1	LZTBLn-0.2	LZTBLn-0.3	LZTBLn-0.4
0.015	16.28	53.85	62.287	64.232	64.813	65.596	66.195
0.02	7.142	24.15	28.638	29.535	29.804	30.167	30.445
0.03	2.41	7.811	9.523	9.823	9.914	10.037	10.131
0.04	1.245	3.607	6.212	6.626	6.903	7.200	7.477
0.05	0.8243	2.065	3.522	3.755	3.910	4.077	4.232
0.06	0.5559	1.369	2.271	2.417	2.513	2.616	2.712
0.08	0.4699	0.7981	1.222	1.293	1.337	1.385	1.430
0.1	0.3968	0.5821	0.822	0.864	0.888	0.914	0.939
0.15	0.3282	0.3978	0.491	0.509	0.517	0.527	0.535
0.2	0.2923	0.3332	0.387	0.399	0.402	0.407	0.411
0.3	0.2498	0.2739	0.304	0.312	0.313	0.315	0.317
0.4	0.2226	0.2411	0.264	0.270	0.271	0.272	0.273
0.5	0.2028	0.2186	0.238	0.243	0.244	0.245	0.245
0.6	0.1838	0.2014	0.219	0.224	0.224	0.225	0.225
0.8	0.1643	0.1763	0.191	0.195	0.195	0.196	0.196
1	0.1477	0.1583	0.171	0.175	0.175	0.176	0.176
1.5	0.1202	0.1288	0.139	0.142	0.142	0.143	0.143
2	0.1037	0.1114	0.120	0.123	0.123	0.123	0.123
3	0.08436	0.09168	0.099	0.101	0.101	0.101	0.101

4	0.07349	0.0809	0.087	0.089	0.089	0.089	0.089
5	0.06656	0.07424	0.079	0.081	0.081	0.082	0.082
6	0.06187	0.06987	0.074	0.076	0.076	0.077	0.077
8	0.05603	0.06472	0.068	0.070	0.070	0.071	0.071
10	0.05269	0.06204	0.065	0.067	0.067	0.068	0.068
15	0.04881	0.05955	0.062	0.064	0.064	0.064	0.065

Table. 3. Calculated values of Linear Attenuation Coefficients using Phy-X/PSD software.

3.3.3. Half value layer (HVL): The half value layer (HVL) values of the prepared LZTBLn glasses were evaluated in the photon energy range of 0.015-15 MeV. Plot between photon energy and half value layer as a function of lanthanum oxide Nps mol% is shown in **Fig. 6.** In the low energy range (0.015-0.05 MeV), the HVL values for the LZTBLn glasses are quite low. At 0.015 MeV, the HVL values lie between 0.010 and 0.011 cm, whereas ordinary concrete and hematite-serpentine show higher values of about 0.042cm and 0.013cm, respectively. The exceptional performance of the prepared glasses in the low energy range is primarily attributed to the predominance of the photoelectric effect, which shows that attenuation is highly dependent on atomic number. In the intermediate energy range (0.1-1 MeV), the HVL values increase gradually. At 0.5 MeV, the HVL values for the prepared glasses range from about 2.83-2.91 cm, while ordinary concrete and hematite–serpentine show higher values of approximately 3.42 cm and 3.17 cm, respectively. This increase is associated with the dominance of Compton scattering, where photon interaction probability decreases compared to the low energy region. In the high-energy region (1-15 MeV), the HVL values increase further and vary slowly with energy. At 15 MeV, the HVL values range from approximately 10.69-11.19 cm for the LZTBLn glasses, compared to 14.16 cm for ordinary concrete and 11.64 cm for hematite–serpentine. Although pair production contributes above 1.022 MeV, the overall attenuation efficiency is lower than at low energies, resulting in higher HVL values. Photon interactions with glass samples are contingent upon the probability of collisions with the atoms within, which influences the attenuation properties [46]. Among all compositions, LZTBLn-0.4 consistently exhibits the lowest HVL values across most energy ranges, confirming that increasing lanthanum oxide content enhances shielding performance. Overall, the prepared LZTBLn glasses shows better radiation shielding efficiency than conventional materials, particularly in the low and intermediate energy regions.

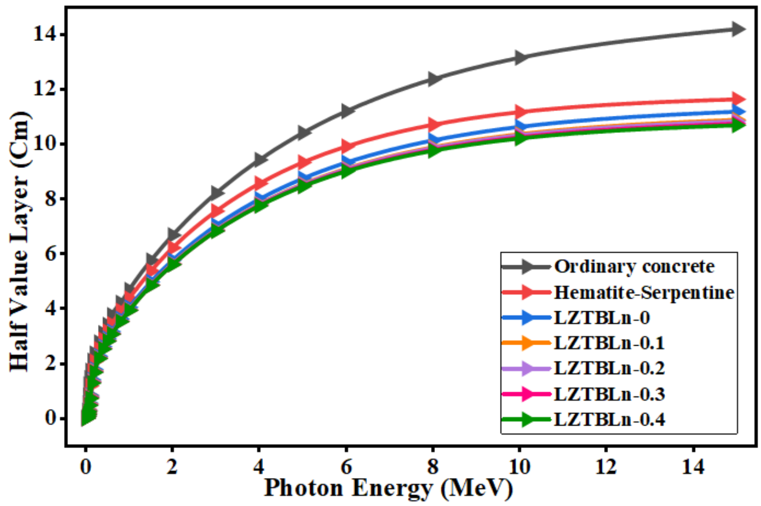

Fig. 6. Variation of Half value layer (HVL) with incident photon energy for Radiation shielding materials

3.3.4. Tenth value layer (TVL): The tenth value layer (TVL) of the prepared LZTBLn glasses was studied in the energy range of 0.015-15 MeV and the values increase as photon energy increases. Plot between photon energy and tenth value layer as a function of lanthanum oxide Nps mol% is shown in **Fig. 7.** In the low energy region that is 0.015 to 0.05 MeV, the TVL values of the LZTBLn glasses are very small. At 0.015 MeV, the TVL values lie between 0.035 and 0.037 cm, whereas ordinary concrete and hematite–serpentine show higher values of about 0.141 cm and 0.043 cm respectively. This indicates enhanced attenuation of the prepared glasses in the low energy range due to the dominance of the photoelectric effect. In the intermediate energy region from 0.1 to 1 MeV, the TVL values increase gradually. At 0.5 MeV, the TVL values of the glasses range from about 9.38 to 9.68 cm, while ordinary concrete and hematite–serpentine exhibit higher values of 11.05 cm and 10.53 cm, respectively. This increase is associated with the dominance of Compton scattering, where photon interaction probability decreases. In the high energy region from 1 to 15 MeV, the TVL values increase further and vary more slowly with energy. At 15 MeV, the TVL values range from 35.52 to 37.16 cm for the LZTBLn glasses, compared to 47.2 cm for ordinary concrete and 38.66 cm for hematite-serpentine. Although pair production contributes at higher energies, the overall attenuation efficiency is lower than in the low energy range, resulting in larger TVL values. Among all samples, LZTBLn-0.4 has the lowest TVL values, indicating better radiation shielding performance with higher lanthanum oxide content [47].

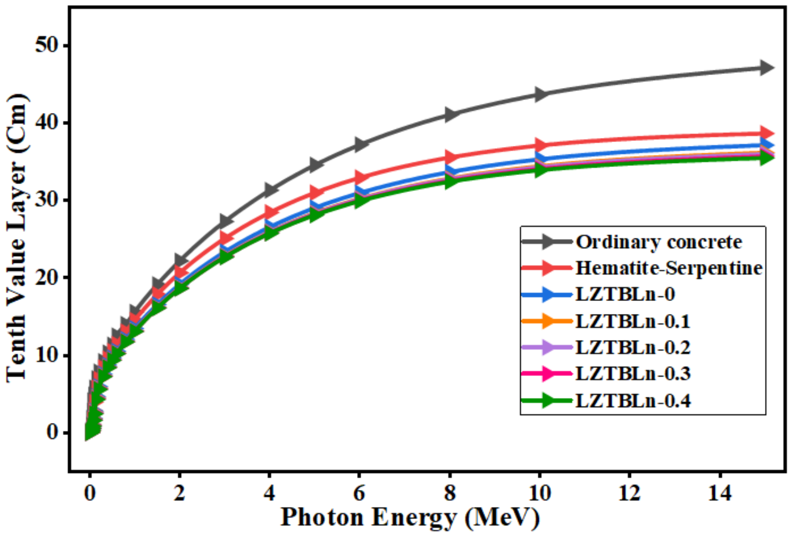

Fig. 7. Variation of Tenth value layer (TVL) with incident photon energy for Radiation shielding materials

3.3.5. Mean free path (MFP): The mean free path values for the prepared LZTBLn glasses were analysed within the photon energy range of 0.015-15 MeV. In the low energy range (0.015-0.05 MeV), the MFP values of the LZTBLn glasses are very small. At 0.015 MeV, the MFP values are around 0.015-0.016 cm, whereas ordinary concrete and hematite–serpentine show higher values of about 0.061 cm and 0.019 cm, respectively. This indicates that photons travel a much shorter distance in the prepared glasses, mainly due to the dominance of the photoelectric effect, which has a high interaction probability at low energies. In the intermediate energy region (0.1-1 MeV), the MFP values increase gradually. At 0.5 MeV, the MFP values for the LZTBLn glasses lie between 4.07 and 4.20 cm, while ordinary concrete and hematite–serpentine exhibit higher values of approximately 4.93 cm and 4.57 cm, respectively. This increase is attributed to the dominance of Compton scattering, where the photon interaction probability decreases compared to the low energy region. In the high energy range (1-15 MeV), the MFP values continue to rise and change gradually with energy. the MFP values range from approximately 15.42-16.14 cm for the LZTBLn glasses, compared to 20.49 cm for ordinary concrete and 16.79 cm for hematite-serpentine. Although pair production contributes above 1.022 MeV, the overall interaction probability remains lower than in the low energy region, leading to larger MFP values. These values were Plot between photon energy mean free path as a function of lanthanum mol% is given in **Fig. 8**. Among all compositions LZTBLn-0.4 generally shows the lowest MFP values across most energy ranges, confirming that increasing lanthanum oxide content enhances photon interaction probability and improves shielding performance [48].

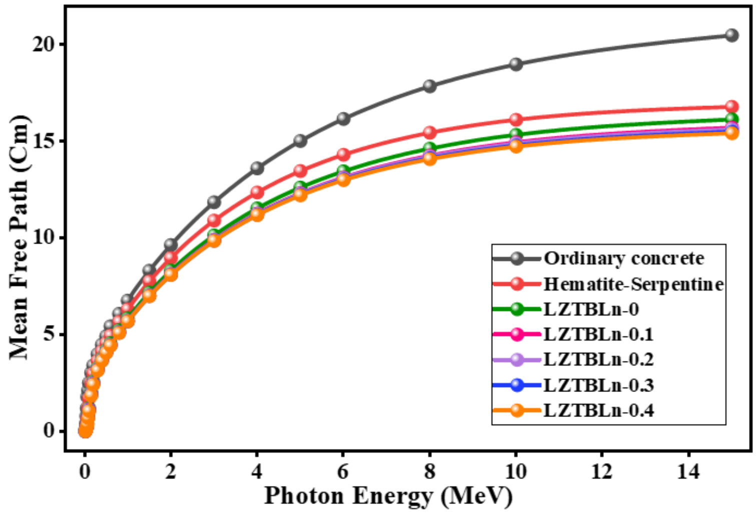

Fig. 8. Variation of Mean free path (MFP) with incident photon energy for Radiation shielding materials

3.3.6. Effective atomic number (Z_{eff}): The effective atomic number for the prepared LZTBLn glasses was analysed across the energy range of 0.015-15 MeV. The calculation of the variation in effective atomic number with photon energy is shown in **Fig. 9**. The values of Z_{eff} increased due to La_2O_3 Nps doping. In the low energy range of 0.015 to 0.05 MeV, the Z_{eff} values are high around 24 to 29, due to the predominance of the photoelectric effect, which has an interaction probability that is significantly proportional to Z^4-Z^5, where Z is the atomic number. In the intermediate energy range of 0.1 to 1 MeV, Z_{eff} decreases to around 8.4 to 10, due to the dominance of Compton scattering, which is mainly depends on electron density and shows a slight dependence on Z. In the high energy range that is above 1 MeV, Z_{eff} increases slightly about 10.5 at 15 MeV due to the contribution of pair production, whose probability is proportional to Z^2. Larger Z_{eff} values reflect a stronger capability to shield from penetrating radiation [49]. Among all samples, LZTBLn-0.4 exhibits the highest Z_{eff} values, suggesting that a higher lanthanum oxide content improves atomic number contribution, enhances radiation interaction and shielding effectiveness.

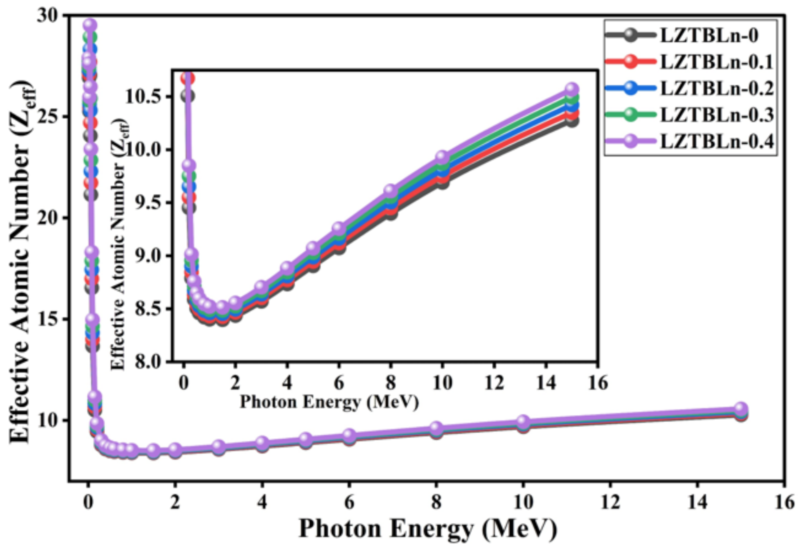

Fig. 9. Variation of Effective atomic number (Z_{eff}) with incident photon energy for LZTBLn glass samples

4. Conclusion:

In this study, quinary $15Li_2O$-$25ZnO$-$2TeO_2$-$(58-x)B_2O_3$-xLa_2O_3 Nps (x = 0-0.4 mol%) Lithium zinc telluroborate (LZTBLn) glasses were successfully synthesized by the conventional melt-quenching technique and their structural, physical, and radiation shielding properties were systematically investigated. The XRD analysis confirmed that the nature of all prepared LZTBLn glasses is amorphous. The incorporation of La_2O_3 nanoparticles led to a gradual increase in density and molecular weight, along with a decrease in molar volume, indicating enhanced packing efficiency and compaction of the glass network. Structural parameters such as reduced polaron radius, decreased inter ionic distance, and increased field strength further confirmed the strengthening of La-O bonds and improved network modification. Using the Phy-X/PSD computational tool, we evaluated radiation shielding parameters, including MAC, LAC, HVL, TVL, MFP, and Z_{eff}, over the photon energy range of 0.015-15 MeV. All glasses showed exceptional attenuation performance in comparison to ordinary concrete and hematite-serpentine, particularly in the low energy region where the photoelectric effect dominates. A consistent enhancement in shielding efficiency was observed with increasing La_2O_3 content, with LZTBLn-0.4 showing the highest MAC, LAC, and Z_{eff} values (LZTBLn-0< LZTBLn-0.1< LZTBLn-0.2< LZTBLn-0.3< LZTBLn-0.4) and the lowest HVL, TVL, and MFP values (LZTBLn-0> LZTBLn-0.1> LZTBLn-0.2> LZTBLn-0.3> LZTBLn-0.4) across most energy ranges. The results clearly demonstrate that La_2O_3 Nps acts as an effective network modifier and significantly improves photon interaction probability. Overall, the prepared LZTBLn glasses, especially with higher lanthanum oxide concentration, are promising candidates for advanced gamma radiation shielding applications.

Acknowledgment:

The authors are thankful for the financial support extended by the Vision Group on Science and Technology (VGST), Government of Karnataka, under the scheme KSTEPS/VGST/ECRA/GRD No. 1251/2023-24

References:

1. Mariselvam, K., & Liu, J. (2021). Investigations on the luminescence and gamma-ray shielding features of Pr^{3+}:BLCZFB glass for orange-red laser and radiation applications. Physics B: Condensed Matter, 614, 413024. https://doi.org/10.1016/j.physb.2021.413024
2. Dong, M., Zhou, S., Xue, X., Sayyed, M. I., Tishkevich, D., Trukhanov, A., & Wang, C. (2022). Study of comprehensive shielding behaviors of chambersite deposit for neutron and gamma ray. Progress in Nuclear Energy, 146, 104155. https://doi.org/10.1016/j.pnucene.2022.104155
3. Al-Hadeethi, Y., & Sayyed, M. I. (2020). Evaluation of gamma-ray shielding characteristics of CaF_2-BaO-P_2O_5 glass system using Phy-X/PSD computer program. Progress in Nuclear Energy, 126, 103397. https://doi.org/10.1016/j.pnucene.2020.103397
4. Poojha, M. K. K., Marimuthu, K., & Teresa, P. E. (2022). Role of modifiers on the structural, mechanical, optical, and radiation protection attributes of Eu^{3+} incorporated

multiconstituent glasses. Nuclear Engineering and Technology, 54, 3841–3848. https://doi.org/10.1016/j.net.2022.05.006

5. Vani, P., Vinitha, G., Sayyed, M. I., Al-Shammari, M., & Manikandan, N. (2021). Effect of rare earth dopants on the radiation shielding properties of barium tellurite glasses. Nuclear Engineering and Technology, 53, 4106-4113. https://doi.org/10.1016/j.net.2021.06.009
6. Hussein, K. I., Alqahtani, M. S., Alzahrani, K. J., Alqahtani, F. F., Zahran, H. Y., Alshehri, A. M., Yahia, I. S., Reben, M., & Yousef, E. S. (2022). The effect of ZnO, MgO, TiO_2, and Na_2O modifiers on the physical, optical, and radiation shielding properties of a TeTaNb glass system. Materials, 15, 1844. https://doi.org/10.3390/ma15051844
7. Alqahtani, M. S., Almarhaby, A. M., Hussein, K. I., AbouDeif, Y. M., Afifi, H., Zahran, H., Yahia, I. S., Grelowska, I., & Yousef, E. S. (2021). Radiation attenuation and photoluminescence properties of host tellurite glasses doped with Er^{3+} ions. Journal of Instrumentation, 16, P01002. https://doi.org/10.1088/1748-0221/16/01/P01002
8. Rammah, Y. S., Al-Buriahi, M. S., El-Agawany, F. I., AbouDeif, Y. M., & Yousef, E. S. (2020). Investigation of mechanical features and gamma-ray shielding efficiency of ternary TeO_2-based glass systems containing Li_2O, Na_2O, K_2O, or ZnO. Ceramics International, 46, 27561–27569. https://doi.org/10.1016/j.ceramint.2020.07.248
9. K.V. Krishnaih, V. Venkatramu, C.K. Jayasankar, Lanthanide-doped tellurite glasses for solar energy harvesting, in: El-Mallawany Raouf (Ed.), Tellurite Glass Smart Materials – Applications in Optics and beyond, Springer, 2018, pp. 249–274, https://doi.org/10.1007/978-3-319-76568-6_11 (Chapter 11).
10. K.U. Kumar, P. Babu, Ch Basavapoornima, R. Praveena, D.S. Rani, C.K. Jayasankar, Spectroscopic properties of Nd^{3+}-doped boro-bismuth glasses for laser applications, Physica B Condens. 646 (2022), 414327, https://doi.org/10.1016/j.physb.2022.414327.
11. G. Lakshminarayana, S.O. Baki, M.I. Sayyed, M.G. Dong, A. Lira, A.S.M. Noora, I. V. Kityk, M.A. Mahdia, Vibrational, thermal features, and photon attenuation coefficients evaluation for TeO_2- B_2O_3- BaO-ZnO-Na_2O-Er_2O_3-Pr_6O_{11} glasses as gammarays shielding materials, J. Non-Cryst. Solids 481 (2018) 568–578, https://doi.org/10.1016/j.jnoncrysol.2017.11.049.
12. Modifier's influence on spectral properties of dysprosium ions doped lead boro-telluro-phosphate glasses for white light applications, Opt Laser. Technol. 156 (2022), 108585, https://doi.org/10.1016/j.optlastec.2022.108585.
13. M.S. Al-Buriahi, C. Eke, S. Alomairy, A. Yildirim, H.I. Alsaeedy, C. Sriwunkum, Radiation attenuation properties of some commercial polymers for advanced shielding applications at low energies, Polym. Adv. Technol. 32 (2021) 2386–2396, https://doi.org/10.1002/pat.5267.
14. T. Kaur, J. Sharma, T. Singh, Feasibility of Pb-Zn binary alloys as gamma, Int. J. Pure Appl. Phys. 13 (2017) 222–225.
15. A.H. Almuqrin, M.I. Sayyed, Radiation shielding characterizations and investigation of TeO_2-WO_3-Bi_2O_3 and TeO_2-WO_3-PbO glasses, Appl. Phys. A 127 (2021) 190, https://doi.org/10.1007/s00339-021-04344-9.

16. V. Chandrappa, Ch Basavapoornima, C.R. Kesavulu, A.M. Babu, S.R. Depuru, C. K. Jayasankar, Spectral studies of Dy^{3+}: zincphosphate glasses for white light source emission applications: a comparative study, J. Non-Cryst. Solids 583 (2022), 121466, https://doi.org/10.1016/j.jnoncrysol.2022.121466.
17. P. Ramprasad, Ch Basavapoornima, S.R. Depuru, C.K. Jayasankar, Spectral investigations of Nd^{3+}:$Ba(PO_3)_2$+La_2O_3 glasses for infrared laser gain media applications, Opt. Mater. 129 (2022), 112482, https://doi.org/10.1016/j. optmat.2022.112482.
18. G. Sathiyapriya, R. Divina, K. Marimuthu, M. Vijayakumar, E. Lacomme, M. I. Sayyed, Exploration on dysprosium ions doped zinc barium boro-tellurite glasses towards radiation screening and photonic applications, Physica B Condens. 612 (2021), 412991, https://doi.org/10.1016/j.physb.2021.412991.
19. S. A. M. Issa, G. Susoy, A. M. Ali, H. O. Tekin, Y. B. Saddeek, A. Al-Hajry, H. Algarni, P. S. Anjana, O. Agar, Applied Physics A **125**, 867 (2019); https://doi.org/10.1007/s00339-019-3169-5
20. Yu. S. Hordieiev, A. V. Zaichuk, Journal of Inorganic and Organometallic Polymers and Materials **33**(2), 591 (2023); https://doi.org/10.1007/s10904-022-02526-3
21. H. Lin, X. Zhao, W. Chen, L. Luo, Journal of Alloys and Compounds **479**, 859–862 (2009); https://doi.org/10.1016/j.jallcom.2009.01.082
22. Maldonado A et al 2021 TeO_2-ZnO-La_2O_3 tellurite glass system investigation for mid infrared robust optical fibers manufacturing J. Alloys Compd. 867 159042
23. Karthika, S., Sundari, S. S., Marimuthu, K., & Meena, P. (2023c). Enhancement of electrical and radiation shielding properties of vanadium doped lithium telluro-borate (LTB) glasses. Chemical Physics Impact, 8, 100430. https://doi.org/10.1016/j.chphi.2023.100430
24. Şakar, E., Özpolat, Ö. F., Alım, B., Sayyed, M., & Kurudirek, M. (2019c). Phy-X / PSD: Development of a user-friendly online software for calculation of parameters relevant to radiation shielding and dosimetry. Radiation Physics and Chemistry, 166, 108496. https://doi.org/10.1016/j.radphyschem.2019.108496
25. Hordieiev, Y. S., & Zaichuk, A. V. (2025c). Lanthanum-doped zinc borate glasses: fabrication, structural analysis, thermal properties, and gamma radiation shielding performance. Journal of Ovonic Research, 21(1), 85–94. https://doi.org/10.15251/jor.2025.211.85
26. Kaur, P., Singh, K., Thakur, S., Singh, P., & Bajwa, B. (2018). Investigation of bismuth borate glass system modified with barium for structural and gamma-ray shielding properties. Spectrochimica Acta Part a Molecular and Biomolecular Spectroscopy, 206, 367–377. https://doi.org/10.1016/j.saa.2018.08.038
27. Kaky, K. M., & Sayyed, M. I. (2023). The radiation shielding parameters of a standard silica glass system. Silicon, 16(3), 1197–1203. https://doi.org/10.1007/s12633-023-02750-7
28. Sayyed, M. I. (2024). Theoretical examination of the radiation shielding qualities of MGO-PBO-SIO2-B_2O_3-BAO glass systems. Silicon, 16(7), 3033–3039. https://doi.org/10.1007/s12633-024-02914-z

29. Gaballah, M., Issa, S. a. M., Saddeek, Y. B., Elsaman, R., Susoy, G., Erguzel, T. T., Alharbi, T., & Tekin, H. O. (2020). Mechanical and nuclear radiation shielding properties of different boro-tellurite glasses: a comprehensive investigation on large Bi_2O_3 concentration. Physica Scripta, 95(8), 085701. https://doi.org/10.1088/1402-4896/ab9bde
30. Thabit, H. A., Ismail, A. K., Hashim, S., Sayyed, M. I., Naseer, K. A., & Bassam, S. A. (2023). Designing High-Density of PBO-Enriched Telluro-Borate glasses for improved radiation shielding: A Comprehensive Study of Attenuation Parameters. ECS Journal of Solid-State Science and Technology, 12(11), 113002. https://doi.org/10.1149/2162-8777/ad06e5
31. Sallam, O., Madbouly, A., Elalaily, N., & Ezz-Eldin, F. (2020). Physical properties and radiation shielding parameters of bismuth borate glasses doped transition metals. Journal of Alloys and Compounds, 843, 156056. https://doi.org/10.1016/j.jallcom.2020.156056
32. El-Khayatt, A. M., Gomaa, H. M., Ebrahem, N. M., & Saudi, H. (2025). Influence of dolomite on the structural, optical, and radiation shielding behavior of Gd/Pb borate glasses: For potential biomedical applications.CeramicsInternational,51(25),44474–44485. https://doi.org/10.1016/j.ceramint.2025.07.177
33. Dong, M., Sayyed, M., Lakshminarayana, G., Ersundu, M. Ç., Ersundu, A., Nayar, P., & Mahdi, M. (2017). Investigation of gamma radiation shielding properties of lithium zinc bismuth borate glasses using XCOM program and MCNP5 code. Journal of Non-Crystalline Solids, 468, 12–16. https://doi.org/10.1016/j.jnoncrysol.2017.04.018
34. Lenkennavar, S. K. (2021). Effect of rare earth impurities on physical, structural and optical properties. Journal of Scientific Research, 65(08), 115–119. https://doi.org/10.37398/jsr.2021.650824
35. M. K. Halimah, W. H. Chiew, H. A. A. Sidek, W. M. Daud, Z. A. Wahab, A. M. Khamirul, S. M. Iskandar, Physical and optical properties of tellurite-based glasses. Sains Malaysiana 43, 889–896 (2014).
36. A. Paul, Chemistry of Glasses, 2nd ed. Chapman & Hall, London (1990).
37. Shelby, J. E. (2020). Introduction to glass science and technology. Royal society of chemistry.
38. Bashter, I. (1997). Calculation of radiation attenuation coefficients for shielding concretes. Annals of Nuclear Energy, 24(17), 1389–1401. https://doi.org/10.1016/s0306-4549(97)00003-0
39. Sayyed, M., Mhareb, M., Alrammah, I., Alghamdi, A. A., Alsurayj, A. A., Alminhali, S. T., Abdelgawad, M. E., Abugurain, Z. A., Alonizan, N., & Alqahtani, M. (2022). Gamma ray shielding and structural properties for TeO_2-BaO-MO modified with Bi_2O_3, TiO_2, MnO_2, MoO_3. Radiation Physics and Chemistry, 205, 110714. https://doi.org/10.1016/j.radphyschem.2022.110714
40. Vani, P., Vinitha, G., Sayyed, M., AlShammari, M. M., & Manikandan, N. (2021). Effect of rare earth dopants on the radiation shielding properties of barium tellurite glasses. Nuclear Engineering and Technology, 53(12), 4106–4113. https://doi.org/10.1016/j.net.2021.06.009

41. Boonin, K., Yasaka, P., Limkitjaroenporn, P., Rajaramakrishna, R., Askin, A., Sayyed, M., Kothan, S., & Kaewkhao, J. (2020). Effect of BaO on lead free zinc barium tellurite glass for radiation shielding materials in nuclear application. Journal of Non-Crystalline Solids, 550, 120386. https://doi.org/10.1016/j.jnoncrysol.2020.120386
42. El-Mallawany, R., El-Agawany, F., Al-Buriahi, Muthuwong, C., Novatski, A., & Rammah, Y. (2020). Optical properties and nuclear radiation shielding capacity of TeO_2-Li_2O-ZnO glasses. Optical Materials, 106, 109988. https://doi.org/10.1016/j.optmat.2020.109988
43. Al-Hadeethi, Y., Sayyed, M., & Tijani, S. (2019). Gamma radiation attenuation properties of tellurite glasses: A comparative study. Nuclear Engineering and Technology, 51(8), 2005–2012. https://doi.org/10.1016/j.net.2019.06.014
44. Kavaz, E., Tekin, H., Kilic, G., & Susoy, G. (2020). Newly developed Zinc-Tellurite glass system: An experimental investigation on impact of Ta_2O_5 on nuclear radiation shielding ability. Journal of Non-Crystalline Solids, 544, 120169. https://doi.org/10.1016/j.jnoncrysol.2020.120169
45. Al-Buriahi, Bakhsh, E. M., Tonguc, B., & Khan, S. B. (2020). Mechanical and radiation shielding properties of tellurite glasses doped with ZnO and NiO. Ceramics International, 46(11), 19078–19083. https://doi.org/10.1016/j.ceramint.2020.04.240
46. Al-Hadeethi, Y., & Sayyed, M. (2019a). The influence of PbO on the radiation attenuation features of tellurite glass. Ceramics International, 45(18), 24230–24235. https://doi.org/10.1016/j.ceramint.2019.08.133
47. Rammah, Y., Özpolat, Ö., Alım, B., Şakar, E., El-Mallawany, R., & El-Agawany, F. (2020). Assessment of gamma-ray attenuation features for La^{+3} co-doped zinc borotellurite glasses. Radiation Physics and Chemistry, 176, 109069. https://doi.org/10.1016/j.radphyschem.2020.109069
48. Karthikeyan, B., & Manikandan, N. (2024). Effect of La_2O_3 on the optical, thermal, structural and radiation shielding properties of TeO_2–ZnO–BaO glasses. Physica Scripta, 99(8), 085926. https://doi.org/10.1088/1402-4896/ad5c13.
49. Al-Buriahi, & Rammah, Y. (2019). Radiation sensing properties of tellurite glasses belonging to ZnO–TeO_2–PbO system using Geant4 code. Radiation Physics and Chemistry, 170, 108632. https://doi.org/10.1016/j.radphyschem.2019.108632